

Article

Research on Compressive and Flexural Properties of Coal Gangue-Slag Geopolymer under Wetting-Drying Cycles and Analysis of Micro-Mechanism

Xiaoyun Yang ^{1,2} , Yan Zhang ^{1,*} , Zhuhan Li ³ and Minglei Wang ¹ 

- ¹ College of Energy and Transportation Engineering, Inner Mongolia Agricultural University, Hohhot 010018, China; ycyangxiaoyun@emails.imau.edu.cn (X.Y.); wangshuoxin@emails.imau.edu.cn (M.W.)
² Department of Civil Engineering, University of Victoria, Victoria, BC V8P 5C2, Canada
³ School of Planning, University of Waterloo, Waterloo, ON N2L 3G1, Canada; z2246li@uwaterloo.ca
* Correspondence: zhangyanli@imau.edu.cn; Tel.: +86-0471-5307514

Abstract: Coal gangue-slag geopolymer is a kind of environment-friendly material with excellent engineering performance and is formed from coal gangue and slag after excitation by an alkaline activator. In this study, three kinds of coal gangue-slag geopolymer were activated by different activators, and the compressive and flexural strengths of water and sulphate solutions in the wetting-drying (W-D) cycles were compared. The microscopic mechanism was analyzed by the XRD, the FTIR and the SEM. The following conclusions are drawn: The influence of W-D cycles on flexural strength was greater than compressive strength. The water migration and the recombination of geopolymers lead to the change of colour, as well as the reduction of flexural strength and compressive strength of geopolymers. The SH geopolymer had excellent anti-erosion ability in terms of flexural strength, and the reason for this was the recombination and polymerization reaction of geopolymer being weaker than the SS and the SSG. The corrosion resistance of the SS was reflected in the compressive strength, because its geopolymerization reaction was fierce, which produced more Na-rich C-N-A-S-H, N-A-S-H and C-A-S-H gels. Therefore, the compressive strength could still reach more than 39 MPa after 150 cycles. Sulfate solution could effectively control the reduction of compressive strength of the SH and the SS geopolymers during W-D cycles. The SSG had the worst corrosion resistance.

Keywords: coal gangue-slag geopolymer; wetting-drying cycles; compressive and flexural strength; micro mechanism



Citation: Yang, X.; Zhang, Y.; Li, Z.; Wang, M. Research on Compressive and Flexural Properties of Coal Gangue-Slag Geopolymer under Wetting-Drying Cycles and Analysis of Micro-Mechanism. *Polymers* **2021**, *13*, 4160. <https://doi.org/10.3390/polym13234160>

Academic Editor: Marta Fernández-García

Received: 19 October 2021
Accepted: 24 November 2021
Published: 28 November 2021

Publisher's Note: MDPI stays neutral with regard to jurisdictional claims in published maps and institutional affiliations.



Copyright: © 2021 by the authors. Licensee MDPI, Basel, Switzerland. This article is an open access article distributed under the terms and conditions of the Creative Commons Attribution (CC BY) license (<https://creativecommons.org/licenses/by/4.0/>).

1. Introduction

A geopolymer is a three-dimensional inorganic polymer with high strength mechanical properties, physical properties, durability, and low carbon dioxide release [1–4]. Geopolymer can be formed quickly by silica aluminum materials (fly ash, slag, coal gangue, red mud, and other solid wastes) excited by alkaline solution [5]. Coal gangue is a by-product of coal, which has negative impacts on the surrounding environment, such as occupation, dust, collapse, landslide, soil erosion, toxic gas, heavy metal pollution, acid water pollution, and so on [6–9]. Coal gangue belongs to the coal-measure kaolinite, and its main chemical composition is SiO₂ and Al₂O₃ [10]. After bleaching, high-temperature calcination, and grinding, coal gangue will be transformed into high-purity kaolin, and it can be transformed into metakaolin when the calcination temperature is controlled in the low-temperature calcination zone, 500–900 °C [11]. Metakaolin is a good raw material for geopolymers [12]. Compared with cement, calcined coal gangue has become the most prospective industrial by-product due to its low carbon footprint [13]. However, geopolymers prepared only with coal gangue as raw materials have a long hardening time and low strength after alkali activation, which limits their wide application in engineering. Ground granulated blast furnace slag (GGBFS) is a highly active powder, and alkali-activated

slag (AAS) is a new type of gelling agent with good mechanical properties and excellent chemical durability [14]. GGBFS can also form high-strength geopolymers after being excited by alkalis [15–17], but its price is relatively expensive, and the large-scale use of slag will increase the cost of geopolymer preparation. The geopolymer produced by the combination of coal gangue and GGBFS can produce high-strength geopolymer in a short time [18,19], and the use of coal gangue as the main material can reduce the cost of preparing geopolymers.

In recent years, extreme weather has occurred frequently. Geopolymers will shrink cracks or decrease strength due to water evaporation or material transformation in high temperature or humid weather [20]. There are few studies available on coal gangue-based geopolymers in dry and wet cycle environments. Whether coal gangue-based geopolymers can adapt to extreme weather conditions has become a problem that must be considered for its wide promotion in engineering. Therefore, the compressive and flexural strength performance of coal gangue-slag geopolymer under dry and wet environments was studied. Water and sulphate resistance were evaluated by appearance, residual compressive strength, and corrosion resistance coefficient (K_f), and the microscopic mechanism was analyzed by X-ray diffractometry (XRD), fourier transform infrared radiation (FTIR), and scanning electron microscopy (SEM).

2. Raw Materials and Methods

Coal gangue and slag powder were obtained from Shanxi Shuguang Coal Coke Group Co.,Ltd. and Hejin city Huaxinyuan Iron and Steel Co.,Ltd., Hejin City, Shanxi Province, China. Activated coal gangue powder is a good raw material for geopolymers. The activation step was used to manually smash the coal gangue into a muffle furnace. Then, it was calcinated at 700 °C for 2 h, and finally crushed to less than 45 μm with an ore crusher. The grade of slag is S95. Figure 1 shows the raw materials.



Figure 1. Raw materials. (a) Raw coal gangue; (b) Slag.

In this experiment, three types of geopolymer were used for a comparative analysis of wetting and drying (W-D) cycles. The three geopolymers are represented by SH, SS, and SSG, respectively. The SH geopolymer was formed by the excitation of 2 mol/L NaOH. The SS geopolymer activator was $\text{Na}_2\text{SiO}_3 + \text{NaOH}$ (18% content, modulus 0.8). The SSG geopolymer activator was desulfurized gypsum + NaOH + Na_2SiO_3 (6% desulfurized gypsum, the content of NaOH + Na_2SiO_3 was 16%, the modulus was 0.6). The preparation of W-D cycle specimens included the following steps. The prepared activator and water were stirred in the magnetic mixer for 30 min. Then, they were poured into the mixer (NJ-160A cement paste mixer, Wuxi Xiyi Building Material Instrument Factory, Wuxi City,

China) together with the coal gangue and slag powder mixture. After mixing, the slurry was poured into the triple mould ($40 \times 40 \times 160 \text{ mm}^3$) according to the standard method, and 60 s shaking was performed on the vibrating table. After that, it was placed in the standard curing box (Humidity is above 95%, the temperature is $20 \pm 2 \text{ }^\circ\text{C}$) for 24 h, the mould was removed, and curing continued for 28 days [21].

The W-D cycles were divided into the water W-D cycles (deionized water) and the sulphate solution (5% Na_2SiO_4) W-D cycles. The strength test result was the average strength of 6 specimens. The total time of each W-D cycle was $(24 \pm 2) \text{ h}$ with following segments: The test piece was soaked in the solution for $(15 \pm 0.5) \text{ h}$, air-dried for 30 min, dried in an oven for 6 h (the temperature of the oven was $(80 \pm 5) \text{ }^\circ\text{C}$), and cooled for 2 h [22]. In the first 75 cycles, the flexural and compressive strength of the test pieces were tested every 15 times. The strength was measured by the automatic bending and compression instrument (WYA-300B, Wuxi Xiyi Building Materials Instrument Factory, Wuxi City, China). After 75 times, the test pieces were tested every 25 times until the end of 150 times. Test termination situation is following: The mass loss rate of W-D cycles reaches 5%. The corrosion resistance coefficient of compressive strength reaches 75%. The calculation method is shown in Equation (1).

$$K_f = \frac{f_{cn}}{f_{c0}} \times 100 \quad (1)$$

where K_f denotes the corrosion resistance coefficient of compressive strength (%); f_{cn} the compressive strength value of specimens corroded by sulphate after N dry-wet cycles (MPa), accurate to 0.1 MPa; f_{c0} the compressive strength value of standard curing specimens at the same age (MPa), accurate to 0.1 MPa.

After completing the strength test, the specimens were crushed and soaked in ethanol for 24 h to terminate the hydration reaction. Then, the powder was dried, and the XRD (D8 Advance, Bruker AXS, Karlsruhe, Germany, the scanning angle is $5^\circ\text{--}90^\circ$, 8° per minute), the SEM (Zeiss Sigma 500, Zeiss, Oberkochen, Germany), and the FTIR (Nicolet iS5, Thermo Fischer Scientific Inc., Waltham, MA, USA) methods were used to analyze the microscopic mechanism.

3. The Appearance of the Specimen

After the W-D cycles, the surface of the test pieces changed in different degrees, and the integrity of the test pieces can be evaluated according to the appearance change. The side and cross-sectional views of the three geopolymers cured for 28 days under standard conditions are shown in Figure 2. The surface of the specimens after 28 days of curing was smooth, the surface was white-blue and dense, and the uniform blue geopolymer was formed on the cross-section.

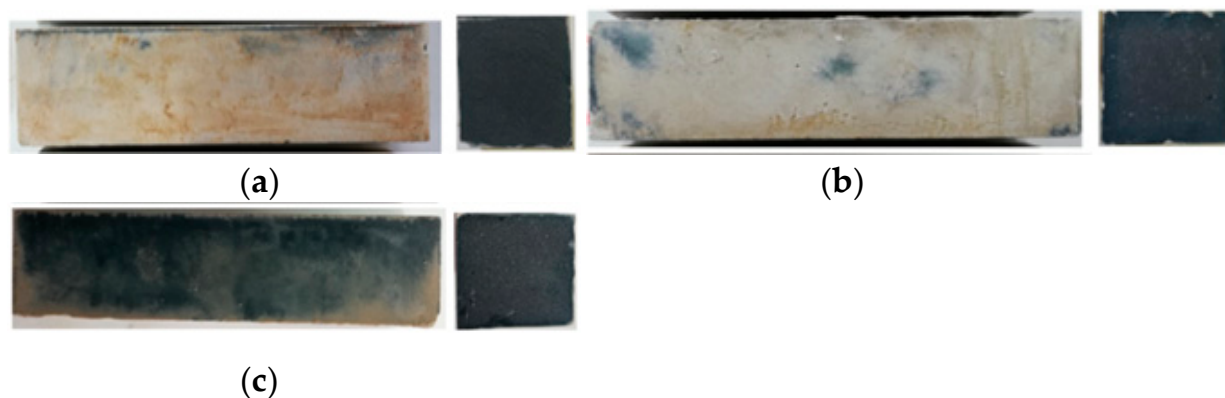


Figure 2. Surface and cross-sectional views of the specimens of standard curing after 28 days. (a) SH geopolymer (b) SS geopolymer (c) SSG geopolymer.

3.1. W-D Cycles of Water

Figure 3 illustrates the surface of the water W-D cycles test pieces. Due to the influence of water cycles, cracks grew on the surface of the specimens, forming grid-like cracks. Few cracks formed on the surface of the SH geopolymer, while SS geopolymer had more cracks on the surface, even some surfaces dropped, and edges were missing. It can be seen from the cross-sectional view that the colour of the geopolymer gradually changed from blue to white after the water W-D cycles, and polycondensation from the outside to the inside occurred.



Figure 3. The surface of specimens after water W-D cycles. (a) SH 150 cycles (b) SS 150 cycles (c) SSG 20 cycles. used than the SH, and the colour of the blue substance was relatively lighter. Some of the SSG specimens began to break into two sections along the cracks at 20 cycles, and this section also showed that the surrounding blue geopolymer turned white.

To observe the polycondensation phenomenon in detail, take the SH and the SS as an example, presented in Figure 4. The surrounding section changed from the original blue geopolymer to white, the white geopolymer evolved from the periphery to the center, and the blue geopolymer in the center began to fade in colour.

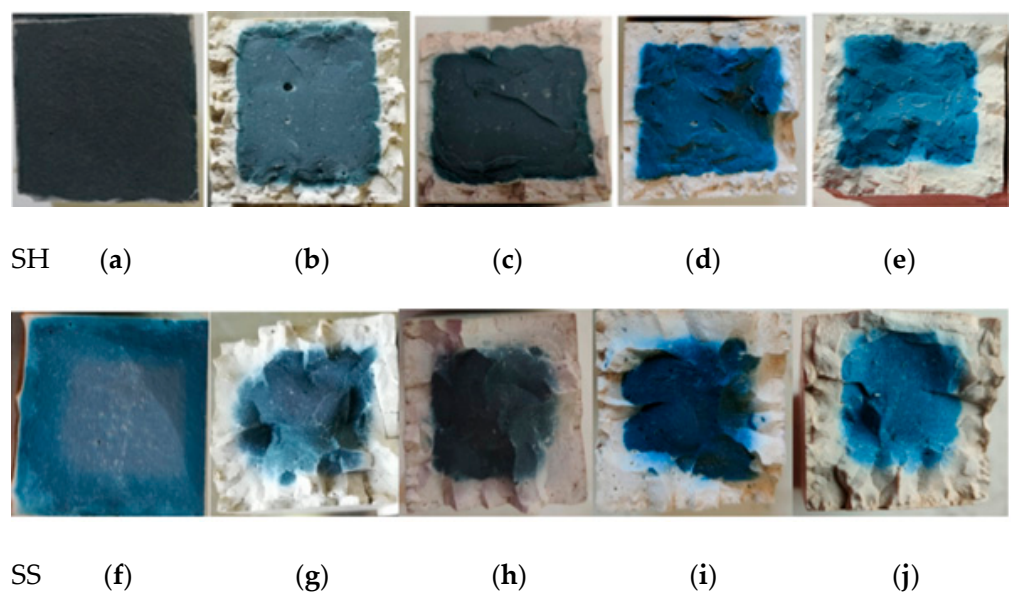


Figure 4. Cross-sectional views of the SH and the SS after water W-D cycles. (a) SH 0 cycles (b) SH 15 cycles (c) SH 30 cycles (d) SH 60 cycles (e) SH 100 cycles (f) SS 0 cycles (g) SS 15 cycles (h) SS 30 cycles (i) SS 60 cycles (j) SS 100 cycles.

3.2. W-D Cycles of Sulphate

All the specimens were corroded, a layer of white sulphate was deposited on the surface, grid cracks appeared, and the external surface peeled off after the sulphate W-D cycles (Figure 5). The blue polycondensation of the SS geopolymer was more obvious, and the change from blue to white around the SH geopolymer was slower. After three cycles, the white geopolymer on the surface of the SSG sample fell off seriously, and the average mass loss rate was 27.3% > 5%. Meanwhile, the entire SSG specimen was crisp, and the flexural strength and compressive strength were only 0.5 MPa and 9.7 MPa ($K_f < 75\%$), respectively. Therefore, the sulphate W-D cycle test of the SSG specimen was terminated, which proved that the SSG geopolymer was not resistant to sulphate corrosion.



Figure 5. Surface and cross-sectional view of the specimens after sulphate W-D cycles. (a) SH 150 cycles (b) SS 150 cycles (c) SSG 3 cycles.

The SH and SS geopolymer are taken as an example to describe the sulphate corrosion process (Figure 6). In the sulphate W-D cycles, a similar situation of the water cycle also occurred, with white geopolymers appearing on the edges and blue geopolymers only in the center of the specimen. Moreover, as the number of cycles increased, the white ceramic materials gradually increased and became denser.

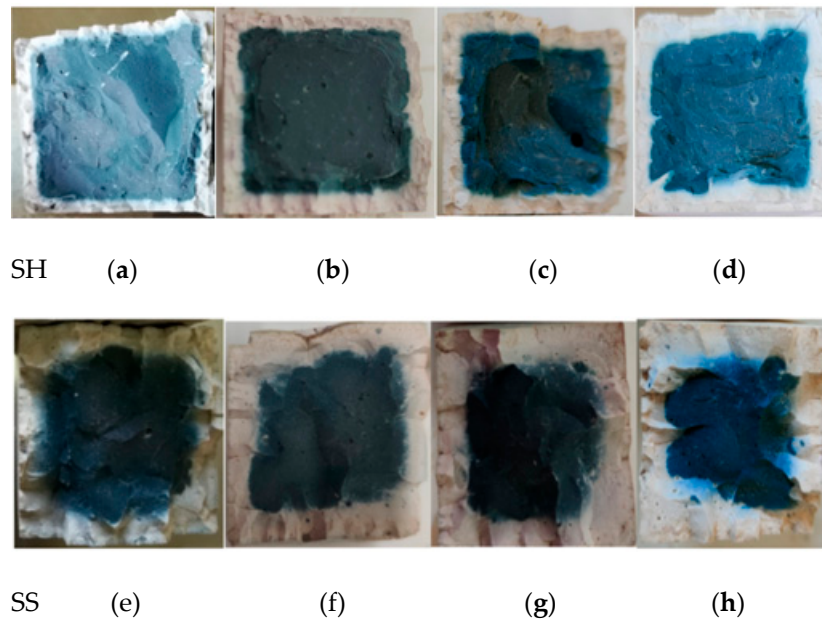


Figure 6. Cross-section of SH and SS geopolymer sulphate W-D cycles. (a) SH 15 cycles (b) SH 30 cycles (c) SH 60 cycles (d) SH 100 cycles (e) SS 15 cycles (f) SS 30 cycles (g) SS 60 cycles (h) SS 100 cycles.

4. Compressive and Flexural Strength Test Results

4.1. W-D Cycles of Water

Figure 7 presents the compressive strength of the water W-D cycles. The SH and the SS showed an increasing trend in the first 60 cycles, before decreasing after 60 cycles. The peak values were 31 MPa and 53.8 MPa, respectively, and the final values were stable at 24 MPa and 39.6 MPa, respectively. Some of the SSG specimens were broken into two pieces along the crack at 20 cycles, and the final compressive strength value was 32.2 MPa.

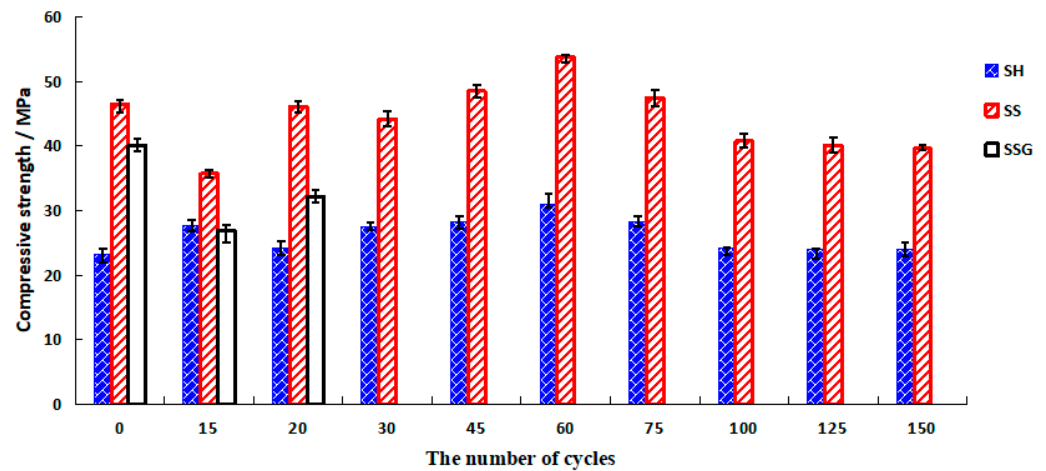


Figure 7. Compressive strength diagram of water W-D cycles.

The curves of the corrosion resistance coefficient after the water W-D cycles ($K_{f\text{ water}}$) are illustrated in Figure 8. The $K_{f\text{ water}}$ of the SH and the SS geopolymers were both above 0.75. The SS geopolymer had the best resistance to water circulation, followed by the SH, and the SSG was the worst. In 20–75 cycles, the $K_{f\text{ water}}$ of the SS geopolymer was greater than 1, which proved that the water W-D cycles were beneficial to improve the compressive strength of SS geopolymer in the early cycles.

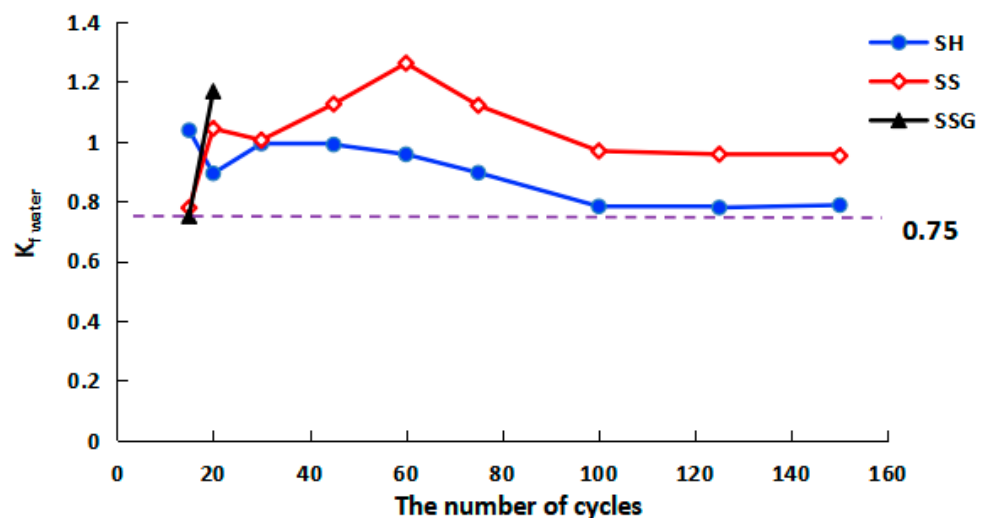


Figure 8. $K_{f\text{ water}}$ curve of compressive strength in water W-D cycles.

Figure 9 shows specimens destroyed along cracks in the flexural test. The flexural strength of water W-D cycles is shown in Figure 10. Flexural strength of the SH increased during the first 30 cycles, then decreased rapidly, and finally stabilized at 2.6 MPa. The SS flexural strength decreased after 15 cycles and stabilized at about 1 MPa after 30 cycles. The SSG had been broken after 20 cycles. Therefore, the flexural resistance of the SH

geopolymer was better than that of the SS geopolymer in water cycles, which was related to its fewer fractures.



Figure 9. Specimen damaged in flexural test.

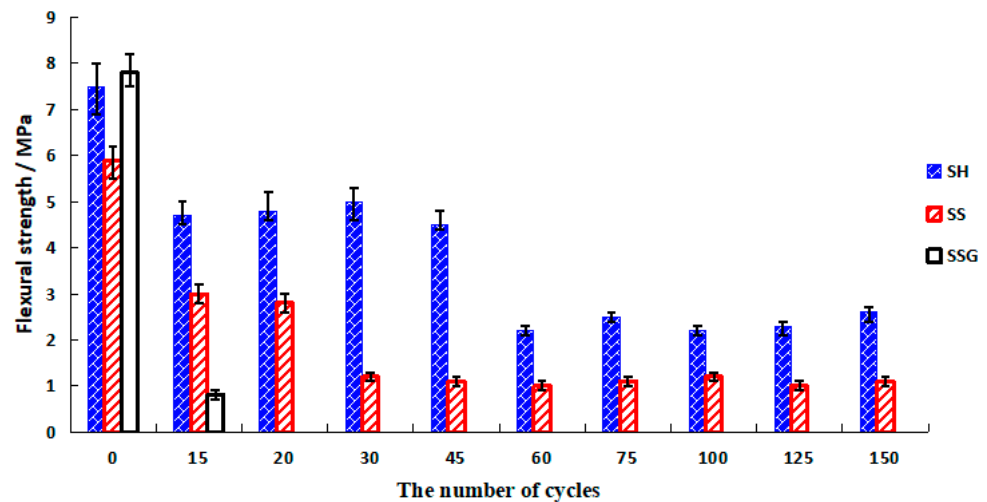


Figure 10. Flexural strength diagram of water W-D cycles.

The specimens under standard curing condition also showed the rule that the flexural strength decreased with the increase of time after 28 days, which proved that the specimens were constantly hardened in the curing process (the compressive strength remained at a high level while the flexural strength decreased) and transformed into brittle materials, and this change process is similar to concrete. The average final flexural strength values of the SH, SS, and SSG specimens without W-D cycles were 4 MPa, 2.7 MPa, and 2.2 MPa, respectively, which were 3.5 MPa, 3.2 MPa, and 5.6 MPa lower than the 28-day flexural strength. Figure 11 describes the flexural strength $K_{f\text{ water}}$ water cycles curve. The $K_{f\text{ water}}$ values of SH were above 0.8 in the early cycles, decreased significantly after 45 cycles, and finally stabilized between 0.5 and 0.6. The $K_{f\text{ water}}$ values of SS dropped faster in the water W-D cycles, and finally stabilized between 0.3 and 0.4. The $K_{f\text{ water}}$ of SSG was only 0.4 at 20 cycles. These results proved that the cracks and the material changes of the W-D cycles had an impact on the specimens.

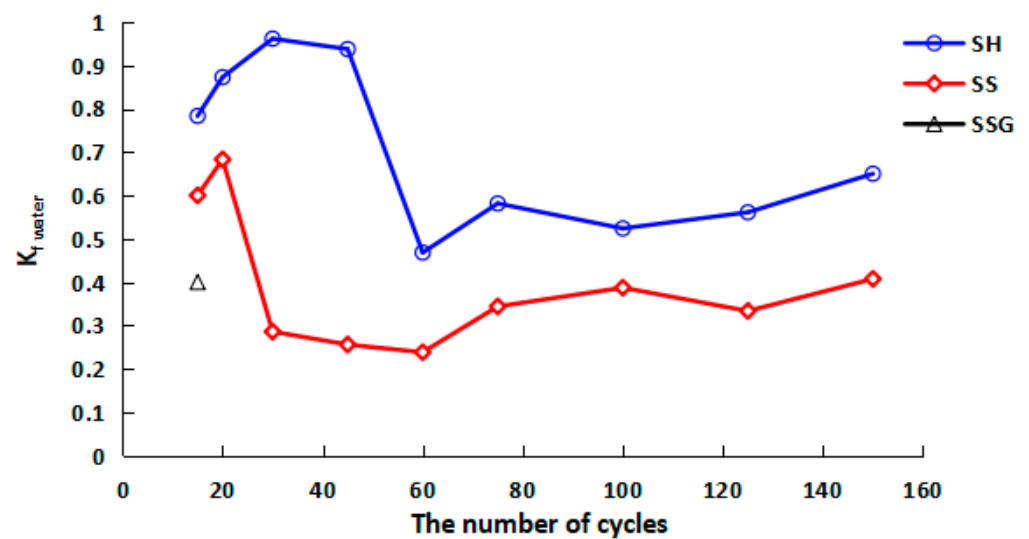


Figure 11. K_{f_water} curve of flexural strength in the water W-D cycles.

4.2. W-D Cycles of Sulphate

Figure 12 shows that the compressive strength of the SH specimens gradually increased before 60 cycles, reaching a maximum of 30.9 MPa, then gradually decreased as the number of cycles increased, and finally stabilized at 26.7 MPa. The compressive strength value of the SS specimen increased during the first 30 cycles, gradually decreased after more than 30 cycles, and finally stabilized at 40.8 MPa. The SSG fractured after three cycles, and the compressive strength was only 9.7 MPa.

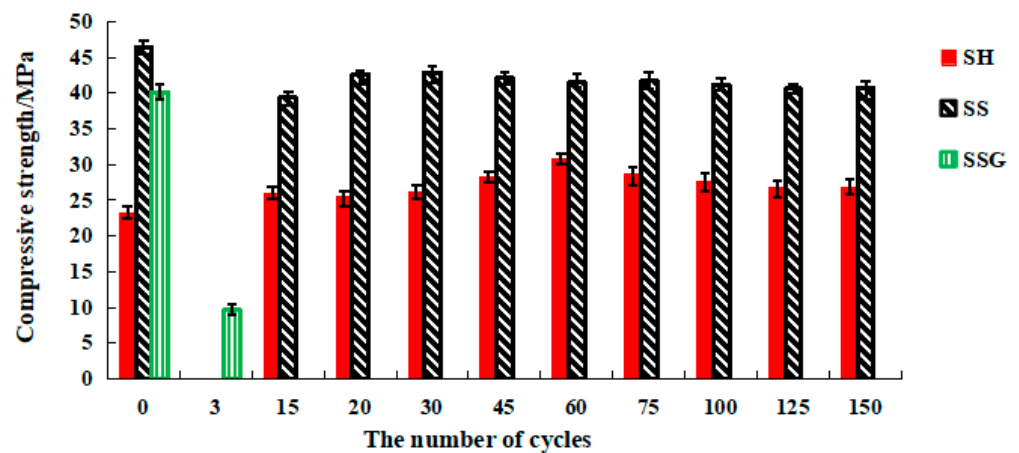


Figure 12. The compressive strength diagram of sulphate W-D cycles.

In Figure 13, the sulphate corrosion resistance coefficient values ($K_{f_sulphate}$) of the SH and the SS geopolymers were greater than 0.75, the $K_{f_sulphate}$ values of the SH geopolymers were above 0.87, and the $K_{f_sulphate}$ values of SS geopolymers were above 0.96. The SS had the best resistance to sulphate corrosion, followed by the SH, and the SSG was the worst.

In Figure 14, the SH geopolymer shows an upward trend between 15 and 30 cycles, which then drops sharply, basically stabilizing between 2.2 and 2.5 MPa. The flexural performance of the SH geopolymer was better than the SS and the SSG geopolymer, mainly because there were fewer cracks during the cycles. The flexural strength of SSG dropped to 0.5 MPa in the third cycle.

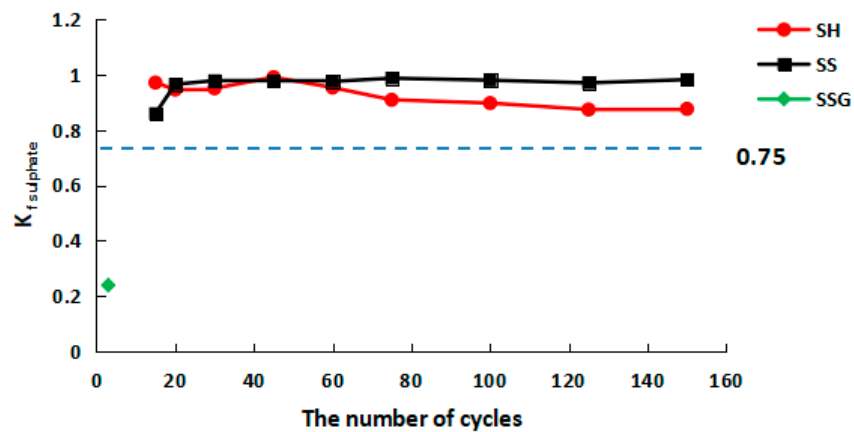


Figure 13. $K_{f_sulphate}$ curve of compressive strength in sulphate W-D cycles.

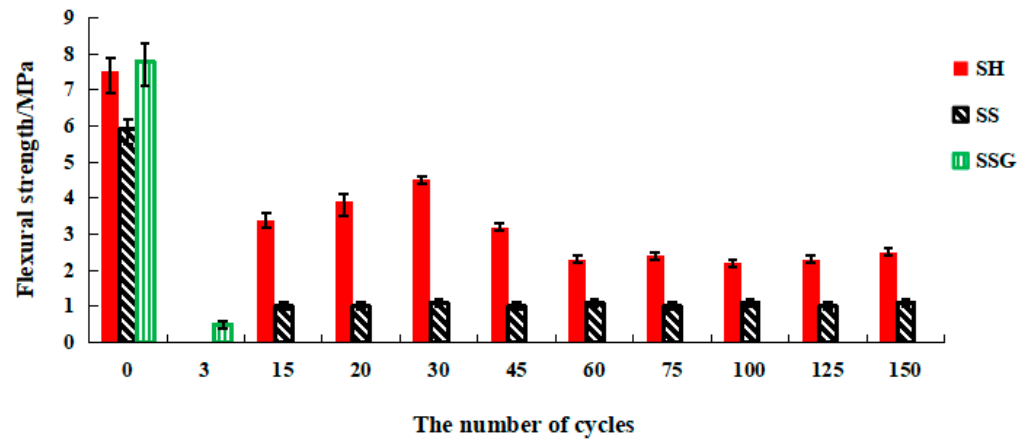


Figure 14. Flexural strength diagram of sulphate W-D cycles.

The change trend of $K_{f_sulphate}$ in the sulfate cycle is described in Figure 15. The sulphate W-D cycles also showed the effect of cracks and hardening on its flexural strength. SH fluctuated greatly in the early stage, showing a trend of first increasing and then decreasing. After 60 cycles, $K_{f_sulphate}$ remained between 0.5 and 0.6. However, SS maintained a relatively stable trend, fluctuating between 0.2 and 0.4. The $K_{f_sulphate}$ of SSG was only 0.07 after three cycles.

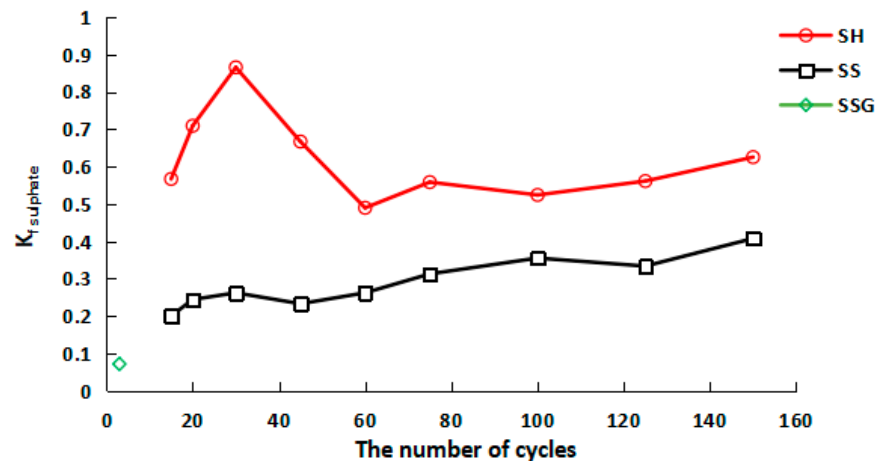


Figure 15. $K_{f_sulphate}$ curve of flexural strength in sulphate W-D cycles.

4.3. Comparative Analysis of the W-D Cycles of Water and Sulphate Solution

The differences in appearance, compressive and flexural strength, and K_f between the water cycles and the sulphate cycles are given in Table 1. The SH geopolymer did not easily form cracks in the W-D cycles, so its flexural strength was higher. The K_f value of the SH geopolymer was lower than that of the SS geopolymer. The SS geopolymer formed cracks more easily, the flexural strength decreased faster, and because of the shallow crack on the surface, it has little effect on the compressive strength. In conclusion, in terms of erosion resistance, the SH geopolymer was superior in terms of flexural strength, while the SS geopolymer was dominant in terms of compressive strength. The SSG had the weakest erosion resistance. The W-D cycles of the sulphate solution were beneficial to inhibit the decrease of the compressive strength of the SH and the SS geopolymers. However, the resistance of the SSG to sulphate erosion was weaker than that of water erosion.

Table 1. Comparison table of various factors of geopolymers.

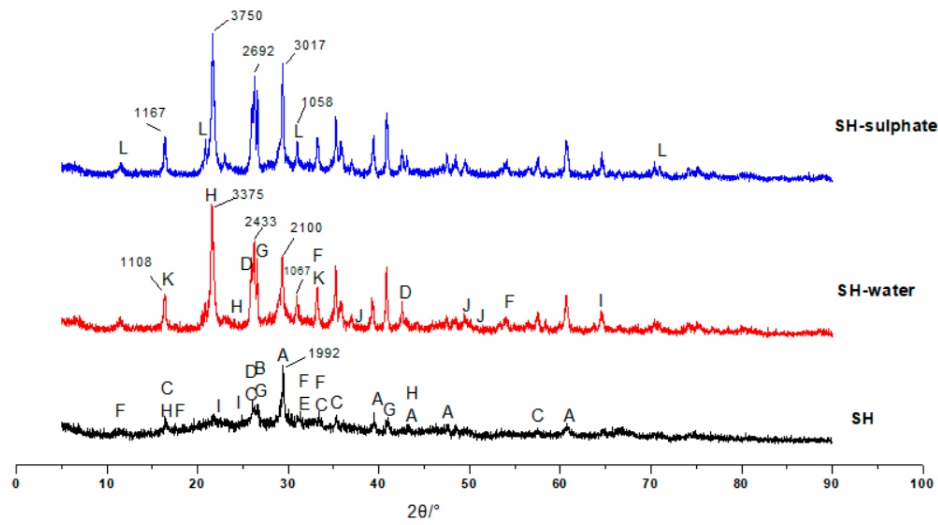
Type	Geopolymer	Cracks	Polycondensation	Cycles	Damage or Ultimate Compressive/Flexural Strength (MPa)	K_f
Water cycles	SH	*	*	150	24/2.6	0.79
	SS	**	**	150	39.6/1.1	0.95
	SSG	***	**	20	32.2/0	-
Sulphate cycles	SH	*	*	150	26.7/2.5	0.88
	SS	**	**	150	40.8/1.1	0.98
	SSG	***	**	3	9.7/0	-

Cracks: Not easy to generate cracks *, easy to generate cracks **, rapid to generate cracks ***. Polycondensation: whiter geopolymers **, less white geopolymer *.

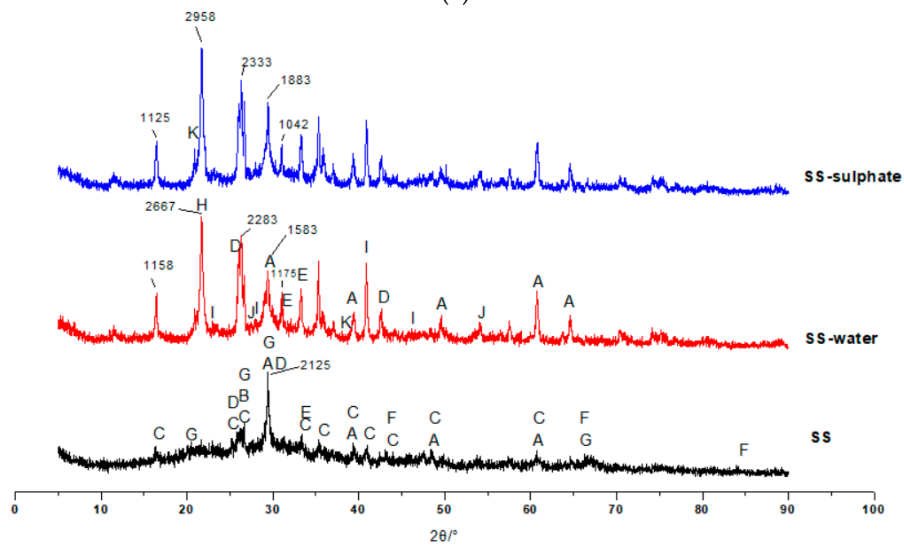
5. Micro Mechanism Analysis

5.1. XRD

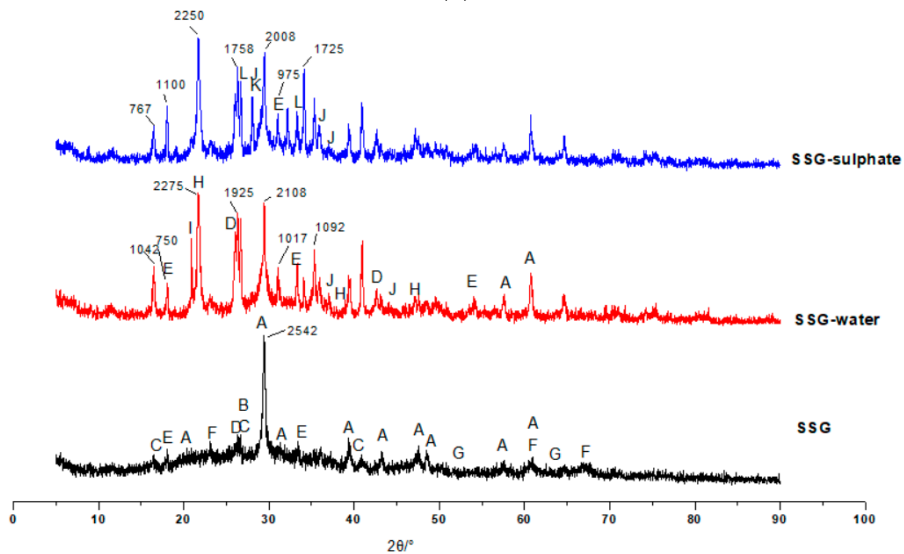
The main hydration products of geopolymers are C-(A)-S-H, N-A-S-H and C-N-A-S-H gels. According to the XRD patterns in Figure 16, the three geopolymers were composed of calcite, silicon dioxide, sillimanite, analcime, gehlenite, zoisite, kyanite, nepheline, and other N-A-S-H and C-A-S-H gels. Among these minerals, nepheline, sillimanite, kyanite, zoisite, and analcime are blue and green, so the colour of the specimens was blue-green (corresponding to Figure 2). After the W-D cycles, the disordered N-A-S-H transforms into a crystalline zeolite phase structure due to drying at a high temperature of 80 °C [23]. From Figure 16, it is clear that all three geopolymers had other characteristic peaks. There were obvious characteristic peaks of Lisetite ($\text{CaNa}_2\text{Al}_4\text{Si}_4\text{O}_{16}$), Labradorite ($\text{Na}_{0.45}\text{Ca}_{0.55}\text{Al}_{1.5}\text{Si}_{2.5}\text{O}_8$), Na-rich Anorthite, Ca-rich Albite, and other C-N-A-S-H gels between 15° and 45°. The characteristic peaks of other minerals were also stronger than those of the samples without the W-D cycles, indicating that the W-D cycles promoted the formation of C-N-A-S-H gel, increased N-A-S-H and C-S-A-H gels, and gypsum products were also present. C-A-S-H and C-N-A-S-H gels are denser and stronger than N-A-S-H gel. The colour of C-N-A-S-H is white, so the specimens had the appearance of white and dense ceramic-like materials, which correspond to the transition from blue substances to white substances in the W-D cycles in Figures 3–6. Meanwhile, this also confirmed the conclusion that the specimen gradually hardened, and the W-D cycles had little influence on the compressive strength of the specimen but a great influence on the flexural strength proposed in Section 4. However, the migration of water and the reorganization of geopolymers formed from the outside to the inside caused cracks on the surface of the specimens and formed a sandwich pattern, resulting in irreversible strength loss.



(a)



(b)



(c)

Figure 16. XRD pattern of coal gangue-slag geopolymer. (a) XRD pattern of the SH geopolymer. A-Calcite B-SiO₂ C-Sillimanite D-Analcime E-Gehlenite F-Zoisite G-Kyanite H-Lisette I-Nepheline J-Labradorite K-Calcium sodium aluminum silicon oxide

L-Gypsum. (b) XRD pattern of the SS geopolymer. A-Calcite B-SiO₂ C-Sillimanite D-Analcime E-Zoisite F-Nepheline G-Kyanite H-Lisette I-Labradorite J-Na-rich Anorthite K-Gypsum. (c) XRD pattern of the SSG geopolymer. A-Calcite B-SiO₂ C-Sillimanite D-Analcime E-Zoisite F-Nepheline G-Labradorite H-Lisette I-Gypsum J-Anorthite K-Ca-rich Albite L-Kyanite.

The products of the sample subjected to the W-D cycles of sulphate solution were similar to those of the water cycle. The peak of calcite after W-D cycles in SH was higher than that of uncycled (Figure 16a), demonstrating that the carbonization strength had increased and Ca²⁺ had not been fully added to the geopolymerization reaction, which corresponded to the appearance of small cracks and small white borders (see Figures 4 and 6). However, the calcite of the SS and the SSG decreased in the W-D cycles compared with that without the cycles (Figure 16b,c), indicating that the W-D cycles reduced the carbonization of the sample, and the excess Ca²⁺ participated in the reaction to generate the C-S-A-H gel and C-N-A-S-H gel. Lisette (C-N-A-S-H gel) peaks were higher in both SH and SS sulphate cycles than in the water cycle, demonstrating that sulphate promoted C-N-A-S-H gel formation, which was consistent with K_f sulphate remaining at a higher level and with less reduction in compressive strength values in sulphate. Desulphurized gypsum was present in the SSG activators, thus introducing Ca²⁺. With a large amount of Ca²⁺ involved in the reaction, more C-A-S-H gel and Ca-rich C-N-A-S-H gel appeared in W-D cycles. In terms of specimen surface contact with the outside world, the severe reaction started from the surface, while the substance in the center of the specimen had no time to react, leading to the peeling from the skin and center. In the sulphate cycles, there were more characteristic peaks of the cementitious material, proving the severe reaction, which corresponded to only three cycles in the sulphate cycles.

5.2. FTIR

In Figure 17, the main peak positions of the characteristic spectral lines of the three geopolymers were the same, indicating that they had similar material compositions. The adsorption zones were located at 3440–3460 cm⁻¹ and 1644–1649 cm⁻¹, which were caused by the OH⁻ tensile vibration and the H–O–H bending vibration caused by the hydration water on the surface of the geopolymer, respectively [24,25]. After the W-D cycles, the intensity of this area decreased and moved to high frequency, which proved that the W-D cycles caused part of the adsorbed water to escape and the crystal structure to collapse. The wavelength of 1426–1447 cm⁻¹ was the O–C–O tensile vibration peak, which was due to the reaction of CO₂ in the air with alkali to form carbonate [26]. After the W-D cycles, the peak strength weakened and moved to the low frequency, which that the group was unstable and the calcium carbonate content decreased, and the W-D cycles inhibited the carbonization reaction. The characteristic strong band at 900–1200 cm⁻¹ reflected the formation of geopolymers, which was related to the asymmetric stretching vibration of T–O–Si (T=Al, Si) formed by TO4 [27,28]. The shift of the frequency band to a lower frequency in this region proved that the polymerization reaction was violent [29]. Therefore, the rate of polymerization of geopolymers in the order of high to low effect is the SS, the SSG, and the SH. In the W-D cycles, the 900–1200 cm⁻¹ region formed two characteristic spectral lines, which proved the vibration and reunion of the T–O–Si bond, and a new phase was formed. Moreover, 1068–1104 cm⁻¹ is the typical position of the main band in the N–A–S–H gel, and 961–969 cm⁻¹ represents the C–A–S–H gel [30]. Therefore, the geopolymer of coal gangue-slag under standard curing conditions was mainly the N–A–S–H gelation, which reflected the geopolymer characteristics of the low calcium system. After the W-D cycles, the C–A–S–H and the C–N–A–S–H gels were generated at high temperature and water loss, which indicated the characteristics of high calcium system geopolymer or Na-rich geopolymer formed after the slag was excited. Further, the wave number moved to a higher wavenumber, illustrating that the group was more stable, and the conversion from amorphous cementation to stable zeolite. In the sulphate solution, because the Na₂SO₄ solution provided an alkaline environment for the geopolymer, the wavenumber moved to a higher wavenumber, and the crystallinity was high. Therefore, the compressive strength

of the geopolymer in the sulphate solution was higher than the compressive strength of the water. The vibrations around $558\text{--}742\text{ cm}^{-1}$ were asymmetric and symmetric vibrations of the Si–O–T bond of the Geopolymer gel of Al4 and SiO₄ tetrahedra [31]. Moreover, $451\text{--}467\text{ cm}^{-1}$ was the bending vibration of Si–O–Si and O–Si–O [27,32].

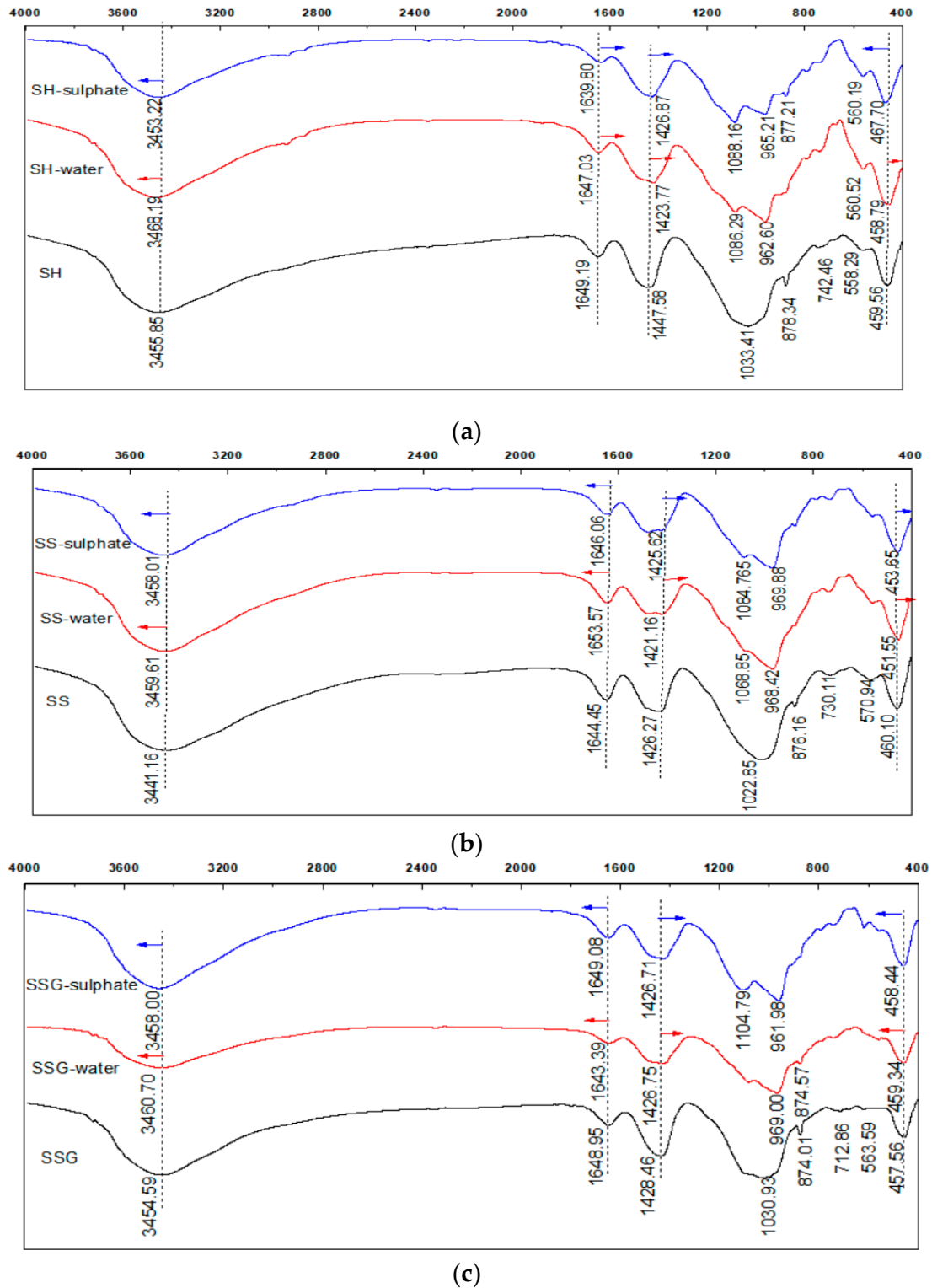


Figure 17. FIRT spectrum of geopolymer. (a) FIRT spectrum of the SH geopolymer. (b) FIRT spectrum of the SS geopolymer. (c) FIRT spectrum of the SSG geopolymer.

5.3. SEM

In Figure 18, it can be seen that C-A-S-H gel, N-A-S-H gel, and C-N-A-S-H gel were formed in the SH, the SS, and the SSG geopolymers. The morphology of geopolymer changed after W-D cycles. The change of shrinkage performance and morphology of geopolymer in a dry environment were caused by the rearrangement and redistribution of C-(A)-S-H, N-A-S-H and C-N-A-S-H nanoparticles over time. The gelled material was more likely to collapse and redistribute after drying, and part of the initial large gel pores was restructured or transformed into smaller pores [20]. This corresponded to the previous conversion from blue to white for denser ceramic materials, as shown in Figures 3–6. Moreover, this change was an irreversible process, resulting in a decrease in strength with the increase of drying times, which corresponded to the decrease of geopolymer strength after the previous W-D cycles.

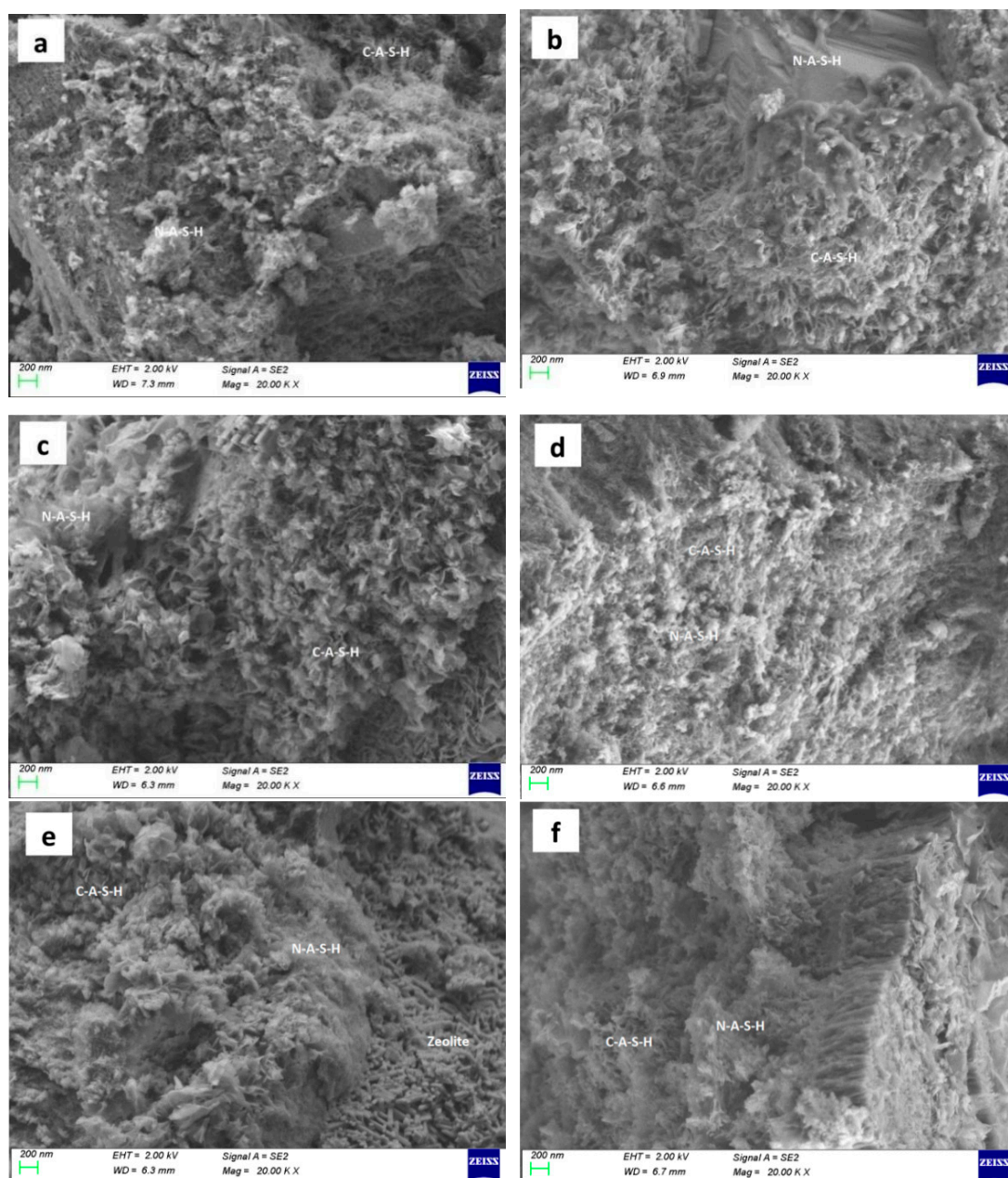


Figure 18. Cont.

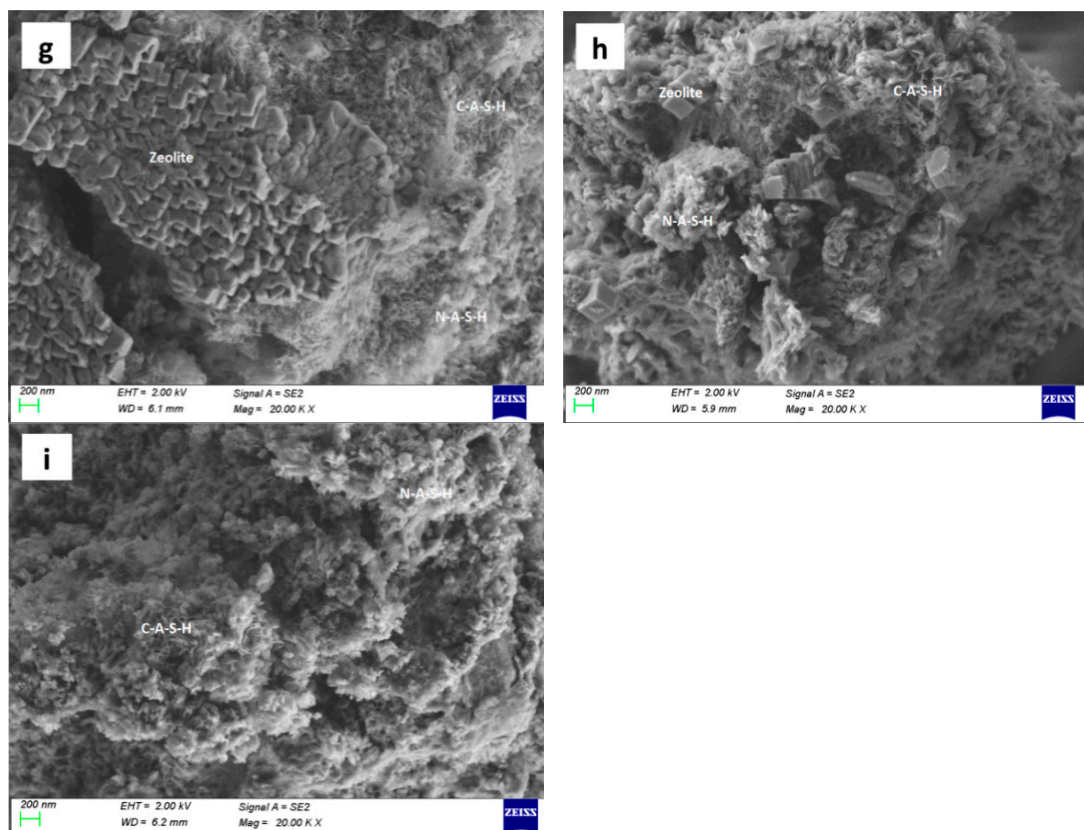


Figure 18. SEM of geopolymers. The magnification is 20KX. ((a) SH (b) SH-water (c) SH-sulphate (d) SS (e) SS-water (f) SS-sulphate (g) SSG (h) SSG-water (i) SSG-sulphate).

Radially shaped and clumped C-A-S-H and N-A-S-H gels are in the SH geopolymer visible in Figure 18a. In Figure 18b,c, after the W-D cycles of the SH geopolymer, the clumped cement-like material was dispersed and collapsed, forming multiple microscopic pores after rearrangement. Figure 18d shows large pieces of dense gel connected in SS geopolymer. Many rod-like zeolite materials could be seen in the SS geopolymer after water W-D cycles (Figure 18e). Geopolymers exhibited stratification after W-D cycles in sulphate solution (Figure 18f). The strength of geopolymer is related to the amount of gel material and zeolite produced. If there are many cementing substances and zeolite generated in the polymerization, the strength of the specimen will be high. SS geopolymer had a large area of interwoven and dense C-A-S-H and N-A-S-H gels and zeolite, so its strength was greater than SH. The reason for this is that the SS alkali activator was Na_2SiO_3 and NaOH solution, Al^{3+} released faster than Si, and enough sodium silicate dissolved aluminum would react with silicon to form oligomeric aluminosilicate, forming sodium aluminosilicate hydrate (N-A-S-H, C-N-A-S-H) gels and zeolites [33].

Figure 18g shows the distribution and arrangement of large flaky zeolite minerals in the SSG geopolymer. The geopolymer had high strength after 28 days of curing under standard curing conditions. However, in W-D cycles, the addition of desulfurized gypsum promoted the exchange and combination of a large amount of Ca^{2+} and Na^+ , and the material forms were rearranged to generate Ca-rich and other C-N-A-S-H cementing materials, forming a network and large agglomerated morphology (Figure 18h,i). Meanwhile, a large number of voids appeared, which was reflected in the decrease in strength.

6. Conclusions

The compressive and flexural strength of the SH, the SS, and the SSG geopolymers under the action of W-D cycles were compared and analyzed. XRD, FTIR, and SEM were used to analyze their mechanism, and the following conclusions are drawn:

- (1) The influence of dry and wet cycles on the flexural strength of geopolymers was greater than the compressive strength. The final sulphate cycle compressive strength of the SH and the SS was higher than that of the water cycle, while the sulphate corrosion resistance of the SSG was weak.
- (2) In terms of compressive strength, the SS geopolymer had stronger erosion resistance than the SH. After 150 cycles of W-D cycling, the SS geopolymer's compressive strength could still reach more than 39 MPa. In terms of flexural strength, the erosion resistance of the SH geopolymer was better than that of the SS, and the compressive strength was more than 2.5 MPa after 150 cycles. The SSG geopolymers had the weakest resistance to erosion.
- (3) In the W-D cycles, the colour change, flexural resistance, and compressive strength of geopolymers were reduced because of the migration of water and the transition of polymerization reaction from the outside to the middle recombination. The SH recombination polymerization reaction is weaker than the SS and the SSG, resulting in fewer cracks and better bending strength. A large amount of zeolite minerals and dense gelling substances were generated in SS, such as Na-rich C–N–A–S–H, so its strength was higher. Because of the presence of desulfurized gypsum in the SS activator, a large amount of Ca^{2+} participated in the reaction to generate Ca-rich C–N–A–S–H, leading to premature external spalling and the most serious erosion.
- (4) The $K_{f \text{ sulphate}}$ of the SH and the SS specimens was higher than the $K_{f \text{ water}}$, which proved that the sulphate solution promoted the hydration reaction in the sulphate cycles, and the C–N–A–S–H gel produced by the recombination reaction was greater than that of the water cycles, which effectively controlled the strength loss. Due to the rapid recombination and polymerization of SSG in the sulphate cycles, the outer skin was detached prematurely from the internal specimen, and the internal specimen was brittle and lost strength under the influence of sulphate crystallization.

Author Contributions: Conceptualization, X.Y.; methodology, X.Y. and Y.Z.; software, X.Y.; validation, X.Y.; formal analysis, X.Y. and Y.Z.; investigation, X.Y.; resources, X.Y. and Y.Z.; data curation, X.Y.; writing—original draft preparation, X.Y.; writing—review and editing, X.Y., Y.Z., Z.L. and M.W.; visualization, X.Y. and M.W.; supervision, Y.Z.; project administration, X.Y. and Y.Z.; funding acquisition, Y.Z. All authors have read and agreed to the published version of the manuscript.

Funding: This research was funded by the National Natural Science Foundation of China (NSFC) (52169023 and 51669025); the China Scholarship Council (202008150091).

Data Availability Statement: The data presented in this study are available on the request from the corresponding author.

Conflicts of Interest: The authors declare that they do not have known competing interests. The funders had no role in the design of the study; in the collection, analyses, or interpretation of data; in the writing of the manuscript, or in the decision to publish the results.

References

1. Zhang, G.-Y.; Ahn, Y.-H.; Lin, R.-S.; Wang, X.-Y. Effect of Waste Ceramic Powder on Properties of Alkali-Activated Blast Furnace Slag Paste and Mortar. *Polymers* **2021**, *13*, 2817. [[CrossRef](#)]
2. Zifang, X.; Xiaotong, Z.; Juan, C. Preparation of Thermal Activation Sludge and Coal Gangue Polymer. *Integr. Ferroelectr.* **2015**, *160*, 1–9. [[CrossRef](#)]
3. Mahmood, A.; Noman, M.T.; Pechočiaková, M.; Amor, N.; Petrů, M.; Abdelkader, M.; Militký, J.; Sozcu, S.; Hassan, S.Z.U. Geopolymers and Fiber-Reinforced Concrete Composites in Civil Engineering. *Polymers* **2021**, *13*, 2099. [[CrossRef](#)] [[PubMed](#)]
4. Kupwade-Patil, K.; Allouche, E.N. Examination of Chloride-Induced Corrosion in Reinforced Geopolymer Concretes. *J. Mater. Civ. Eng.* **2013**, *25*, 1465–1476. [[CrossRef](#)]
5. Quiatchon, P.R.J.; Dollente, I.J.R.; Abulencia, A.B.; Libre, R.G.D.G.; Villoria, M.B.D.; Guades, E.J.; Promentilla, M.A.B.; Ongpeng, J.M.C. Investigation on the Compressive Strength and Time of Setting of Low-Calcium Fly Ash Geopolymer Paste Using Response Surface Methodology. *Polymers* **2021**, *13*, 3461. [[CrossRef](#)]
6. Zhao, Y.; Qiu, J.; Ma, Z.; Sun, X. Eco-friendly treatment of coal gangue for its utilization as supplementary cementitious materials. *J. Clean. Prod.* **2021**, *285*, 124834. [[CrossRef](#)]

7. Jabłońska, B.; Kityk, A.V.; Busch, M.; Huber, P. The structural and surface properties of natural and modified coal gangue. *J. Environ. Manag.* **2017**, *190*, 80–90. [[CrossRef](#)] [[PubMed](#)]
8. Huang, Y.; Zhang, J.; Yin, W.; Sun, Q. Analysis of Overlying Strata Movement and Behaviors in Caving and Solid Backfilling Mixed Coal Mining. *Energies* **2017**, *10*, 1057. [[CrossRef](#)]
9. Guan, J.; Lu, M.; Yao, X.; Wang, Q.; Wang, D.; Yang, B.; Liu, H. An Experimental Study of the Road Performance of Cement Stabilized Coal Gangue. *Crystals* **2021**, *11*, 993. [[CrossRef](#)]
10. Gao, X.; Liu, C.; Shui, Z.; Yu, R. Effects of Expansive Additives on the Shrinkage Behavior of Coal Gangue Based Alkali Activated Materials. *Crystals* **2021**, *11*, 816. [[CrossRef](#)]
11. Li, Z.; Gao, Y.; Zhang, J.; Zhang, C.; Chen, J.; Liu, C. Effect of particle size and thermal activation on the coal gangue based geopolymer. *Mater. Chem. Phys.* **2021**, *267*, 124657. [[CrossRef](#)]
12. Cremona, C.; Vildaer, S.; Cadillac, M. Experimental Study of Blended Binders with Metakaolin. *Sustainability* **2021**, *13*, 10548. [[CrossRef](#)]
13. Yi, C.; Ma, H.; Zhu, H.; Li, W.; Xin, M.; Liu, Y.; Guo, Y. Study on chloride binding capability of coal gangue based cementitious materials. *Constr. Build. Mater.* **2018**, *167*, 649–656. [[CrossRef](#)]
14. Juenger, M.C.G.; Winnefeld, F.; Provis, J.L.; Ideker, J.H. Advances in alternative cementitious binders. *Cem. Concr. Res.* **2011**, *41*, 1232–1243. [[CrossRef](#)]
15. Zhao, Y.; Shi, T.; Cao, L.; Kan, L.; Wu, M. Influence of steel slag on the properties of alkali-activated fly ash and blast-furnace slag based fiber reinforced composites. *Cem. Concr. Compos.* **2021**, *116*, 103875. [[CrossRef](#)]
16. Saludung, A.; Azeyanagi, T.; Ogawa, Y.; Kawai, K. Effect of silica fume on efflorescence formation and alkali leaching of alkali-activated slag. *J. Clean. Prod.* **2021**, *315*, 128210. [[CrossRef](#)]
17. Algaifi, H.A.; Mustafa Mohamed, A.; Alsuhaibani, E.; Shahidan, S.; Alrshoudi, F.; Huseien, G.F.; Bakar, S.A. Optimisation of GBFS, Fly Ash, and Nano-Silica Contents in Alkali-Activated Mortars. *Polymers* **2021**, *13*, 2750. [[CrossRef](#)]
18. Ma, H.; Zhu, H.; Wu, C.; Fan, J.; Yang, S.; Hang, Z. Effect of shrinkage reducing admixture on drying shrinkage and durability of alkali-activated coal gangue-slag material. *Constr. Build. Mater.* **2021**, *270*, 121372. [[CrossRef](#)]
19. Liu, C.S.; Zhong, H.; Gao, X.; Ma, S. Performance evaluation of alkali-activated coal gangue-blast furnace slag composite. *Bull. Chin. Ceram. Soc.* **2020**, *39*, 2877–2884. [[CrossRef](#)]
20. Ye, H.; Radlińska, A. Shrinkage mechanisms of alkali-activated slag. *Cem. Concr. Res.* **2016**, *88*, 126–135. [[CrossRef](#)]
21. International Organization for Standardization. *ISO 679:2009(E) Cement-Test Methods-Determination of Strength*; International Standards Organization: Geneva, Switzerland, 2009.
22. Ministry of Housing and Urban-Rural Development of the People's Republic of China. *G.T. 50082-2009 Standard for Test Methods of Long-Term Performance and Durability of Ordinary Concrete*; China Architecture & Building Press: Beijing, China, 2009.
23. Rovnaník, P. Effect of curing temperature on the development of hard structure of metakaolin-based geopolymer. *Constr. Build. Mater.* **2010**, *24*, 1176–1183. [[CrossRef](#)]
24. Aredes, F.G.M.; Campos, T.M.B.; Machado, J.P.B.; Sakane, K.K.; Thim, G.P.; Brunelli, D.D. Effect of cure temperature on the formation of metakaolinite-based geopolymer. *Ceram. Int.* **2015**, *41*, 7302–7311. [[CrossRef](#)]
25. Huang, X.; Zhuang, R.; Muhammad, F.; Yu, L.; Shiau, Y.; Li, D. Solidification/stabilization of chromite ore processing residue using alkali-activated composite cementitious materials. *Chemosphere* **2017**, *168*, 300–308. [[CrossRef](#)] [[PubMed](#)]
26. Zhao, S.; Muhammad, F.; Yu, L.; Xia, M.; Huang, X.; Jiao, B.; Lu, N.; Li, D. Solidification/stabilization of municipal solid waste incineration fly ash using uncalcined coal gangue-based alkali-activated cementitious materials. *Environ. Sci. Pollut. Res.* **2019**, *26*, 25609–25620. [[CrossRef](#)]
27. Kaya, K.; Soyer-Uzun, S. Evolution of structural characteristics and compressive strength in red mud–metakaolin based geopolymer systems. *Ceram. Int.* **2016**, *42*, 7406–7413. [[CrossRef](#)]
28. Phair, J.W.; Van Deventer, J.S.J. Effect of the silicate activator pH on the microstructural characteristics of waste-based geopolymers. *Int. J. Miner. Process.* **2002**, *66*, 121–143. [[CrossRef](#)]
29. Heikal, M.; Nassar, M.Y.; El-Sayed, G.; Ibrahim, S.M. Physico-chemical, mechanical, microstructure and durability characteristics of alkali activated Egyptian slag. *Constr. Build. Mater.* **2014**, *69*, 60–72. [[CrossRef](#)]
30. Garcia-Lodeiro, I.; Palomo, A.; Fernández-Jiménez, A.; Macphee, D.E. Compatibility studies between N-A-S-H and C-A-S-H gels. Study in the ternary diagram $\text{Na}_2\text{O}-\text{CaO}-\text{Al}_2\text{O}_3-\text{SiO}_2-\text{H}_2\text{O}$. *Cem. Concr. Res.* **2011**, *41*, 923–931. [[CrossRef](#)]
31. Sore, S.O.; Messan, A.; Prud'homme, E.; Escadeillas, G.; Tsobnang, F. Synthesis and characterization of geopolymer binders based on local materials from Burkina Faso–Metakaolin and rice husk ash. *Constr. Build. Mater.* **2016**, *124*, 301–311. [[CrossRef](#)]
32. Ye, N.; Yang, J.; Ke, X.; Zhu, J.; Li, Y.; Xiang, C.; Wang, H.; Li, L.; Xiao, B. Synthesis and Characterization of Geopolymer from Bayer Red Mud with Thermal Pretreatment. *J. Am. Ceram. Soc.* **2014**, *97*, 1652–1660. [[CrossRef](#)]
33. Duxson, P.; Fernández-Jiménez, A.; Provis, J.L.; Lukey, G.C.; Palomo, A.; van Deventer, J.S.J. Geopolymer technology: The current state of the art. *J. Mater. Sci.* **2007**, *42*, 2917–2933. [[CrossRef](#)]